Vacuum 198 (2022) 110852

Contents lists available at ScienceDirect

Vacuum

journal homepage: www.elsevier.com/locate/vacuum

Study of craters formed on surface of AISI 321 stainless steel after high power ion-beam exposure

Mikhail V. Zhidkov [a,c,*], Alexander E. Ligachev [b], Evgeniy V. Golosov [c], Marina Y. Gazizova [a], Sergey K. Pavlov [d], Gennadiy E. Remnev [d]

[a] Belgorod State National Research University, 85 Pobedy Str, Belgorod, 308015, Russia
[b] Prokhorov Institute of General Physics RAS, 38 Vavilova Str, Moscow, 119991, Russia
[c] Institute of Problems of Chemical Physics of RAS, Ac. Semenov Avenue 1, Chernogolovka, Moscow Region, 142432, Russia
[d] Tomsk Polytechnic University, Lenina Avenue 30, Tomsk, 634050, Russia

ARTICLE INFO

Keywords:
AISI 321 stainless steel
High-power ion beam (HPIB)
Crater

ABSTRACT

Surface topography and elemental composition of craters formed on the surface of AISI 321 stainless steel after processing with powerful pulsed flows of C^{n+} and H^{+} ions (accelerating voltage: 250 keV, pulse duration: approximately 100 ns) are studied. Processing is performed using single-pulse fluences of 1 and 3 J/cm^2, with the number of pulses ranging from 1 to 50. It is determined that the average size of the craters increases and the number of craters decreases with an increase in the number of impact pulses. The average size and number of craters are not dependent on the degree of preliminary deformation of the samples. Based on the applied processing parameters, it is established that titanium sulfide or titanium carbosulfide inclusions are the preferred crater sites. Furthermore, the crater structure is examined through electron backscatter diffraction analysis. The structure and phase composition of the craters formed on steel as a result of exposure to a pulsed ion beam do not differ from the structural-phase state of the crater-free regions.

1. Introduction

Although processing with a high-power ion beam (HPIB) increases the hardness, wear resistance, corrosion resistance, and fatigue life of materials [1–3], many studies have demonstrated that this type of exposure leads to the formation of unique surface defects, such as craters. This is detrimental because pores, holes, or microcracks can form in the center of the crater, which in turn can function as stress concentrators and are potential sources of corrosion and locations for fatigue crack formation [4]. To minimize the negative impact of craters, it is critical to study the crater formation mechanism as well as the peculiarities of their formation.

The craters formed after HPIB exposure on AISI 4260 steel [5], copper [6], magnesium [7], and titanium and its alloys [8–10] have been experimentally studied. Although many possible mechanisms for crater formation have been proposed [11–13], they still are a subject of discussion.

Fe–Cr–Ni austenitic stainless steels are the most common multicomponent construction materials used in engineering, chemical, petrochemical, and nuclear industries [14]. These steels have good mechanical, fabrication, and corrosion-resistance properties. In this study, we examine the structural phase features of the craters formed on the surface of AISI 321 austenitic stainless steel after HPIB exposure through scanning electron microscopy and X-ray diffraction analysis.

2. Materials and methods

AISI 321 stainless steel containing 0.12% C, 18% Cr, 10% Ni, and 0.5% Ti (wt.%) was used for the experiments.

Before surface processing with a HPIB, the samples were mechanically polished to a “mirror finish” on a LaboPol-20 machine (Struers). Irradiation was performed with a TEMP accelerator, which involved the flow of carbon ions (C^{n+}) ions and protons (H^{+}) with a singly-charged-ion energy of 250 keV and pulse duration of approximately 100 ns [15]. Single-pulse fluences (F) of 1 and 3 J/cm^2 were applied and the number of pulses was varied from 1 to 50.

The topography and elemental composition of the near-surface layer of the samples were studied through scanning electron microscopy

* Corresponding author. Belgorod State National Research University, 85 Pobedy Str, Belgorod, 308015, Russia.
E-mail addresses: zhidkov@bsu.edu.ru (M.V. Zhidkov), golosov@icp.ac.ru (E.V. Golosov), remnev06@mail.ru (G.E. Remnev).

https://doi.org/10.1016/j.vacuum.2021.110852
Received 7 September 2021; Received in revised form 10 November 2021; Accepted 22 December 2021
Available online 24 December 2021

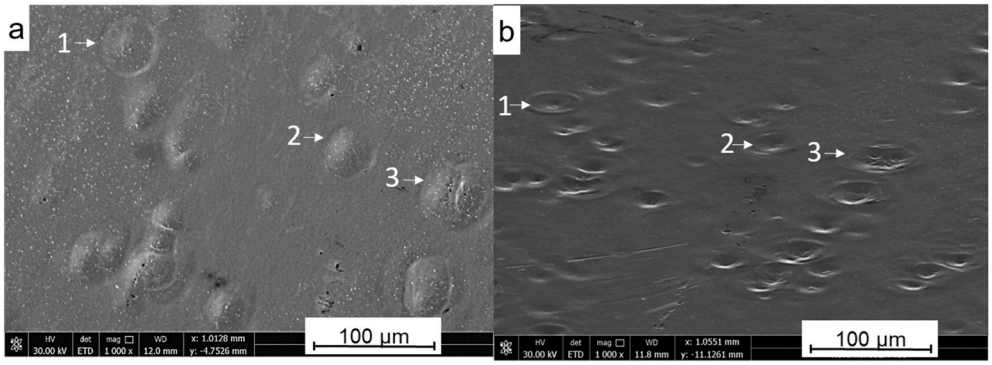

Fig. 1. Appearance of craters on the surface of AISI 321 steel after HPIB processing (F = 3 J/cm^2, five pulses): a) without tilting the sample in the microscope column and b) by tilting the sample in the microscope column by 70°. For ease of visualization, locations of some of the craters before and after tilting are indicated by the numbers in white.

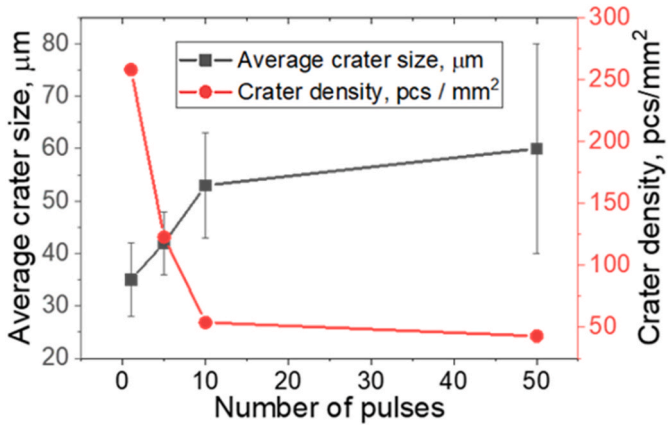

Fig. 2. Dependence of the average size and number of craters on AISI 321 steel on the number of HPIB pulses at F = 3 J/cm^2.

(SEM) using an FEI Quanta 600 microscope equipped with an EDAX energy-dispersion spectrometer (spectrometer resolution: 127.1 eV (Mn K_α), element: Be) and an FEI Nova NanoSem 450 microscope. The surface structure was investigated through electron backscatter diffraction (EBSD) analysis, whereas the phase composition was investigated using an ARL X'TRA diffractometer with Cu K_α radiation in the Bragg-Brentano focusing mode.

The thin foil, which was cut from the cross section of the crater by ionic thinning of the crater material with a focused ion-beam on a FEI Helios 660 scanning electron microscope, was examined using a Tecnai G2 20F S-T (FEI) transmission electron microscope (TEM).

3. Results and discussion

3.1. Surface topography

Typically, the resulting craters (Fig. 1) have central symmetry, but their size, shape, and number (density per unit of irradiated surface) vary significantly depending on the processing parameters, namely, the energy density and number of pulses. The craters can be double or triple, forming extended surface defects; they can be clearly or barely visible and only detectable when the sample is tilted in the microscope column (Fig. 1b). For a fluence (F) of 1 J/cm^2 or 3 J/cm^2, the average size of the craters increases and their number decreases with an increase in the number of pulses (Fig. 2).

For studying the effect of the initial phase composition of steel on the crater formation process, a series of samples were deformed with varying degrees of reduction (25–75%) by cold rolling. The cold plastic-deformation of the austenitic steel (γ-Fe) resulted in refinement of the grain structure and formation of α-Fe. The diffraction patterns of the steel samples and the phase distribution maps of the deformed samples before HPIB processing are depicted in Fig. 3. The phase composition of the steel samples and HPIB irradiation parameters are given in Table 1.

Table 1
Phase composition of the steel samples and irradiation modes used in experiment.

Cold reduction, %	α-Fe content, %	HPIB processing parameters	
		Fluece, J/cm^2	Number of pulses
25	16	1, 3	1, 10, 50
50	40		
75	81		

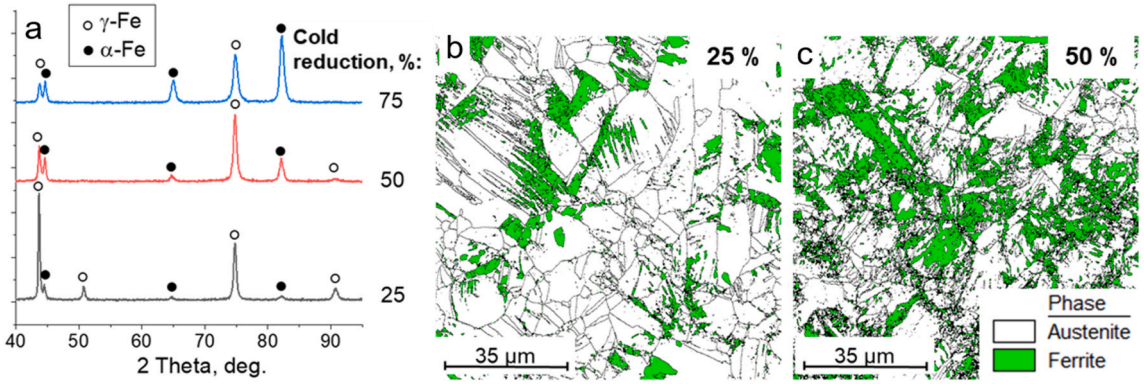

Fig. 3. (a) Diffraction patterns and (b, c) phase distribution maps (before HPIB processing).

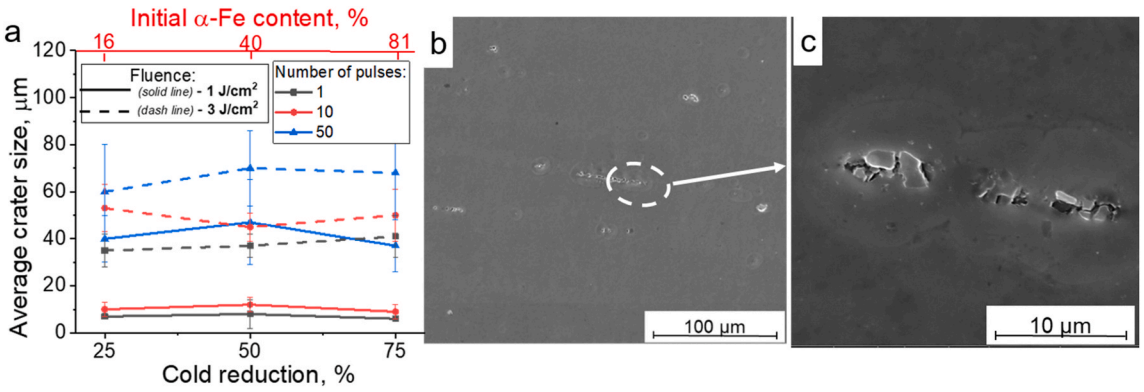

Fig. 4. a) Dependence of the average crater size on the number of HPIB pulses and the initial α-Fe content of the samples at F = 1 J/cm^2 (b, c) Elongated craters on the surface of AISI 321 steel (cold reduction 50%) after HPIB processing (F = 1 J/cm^2, 1 impulse).

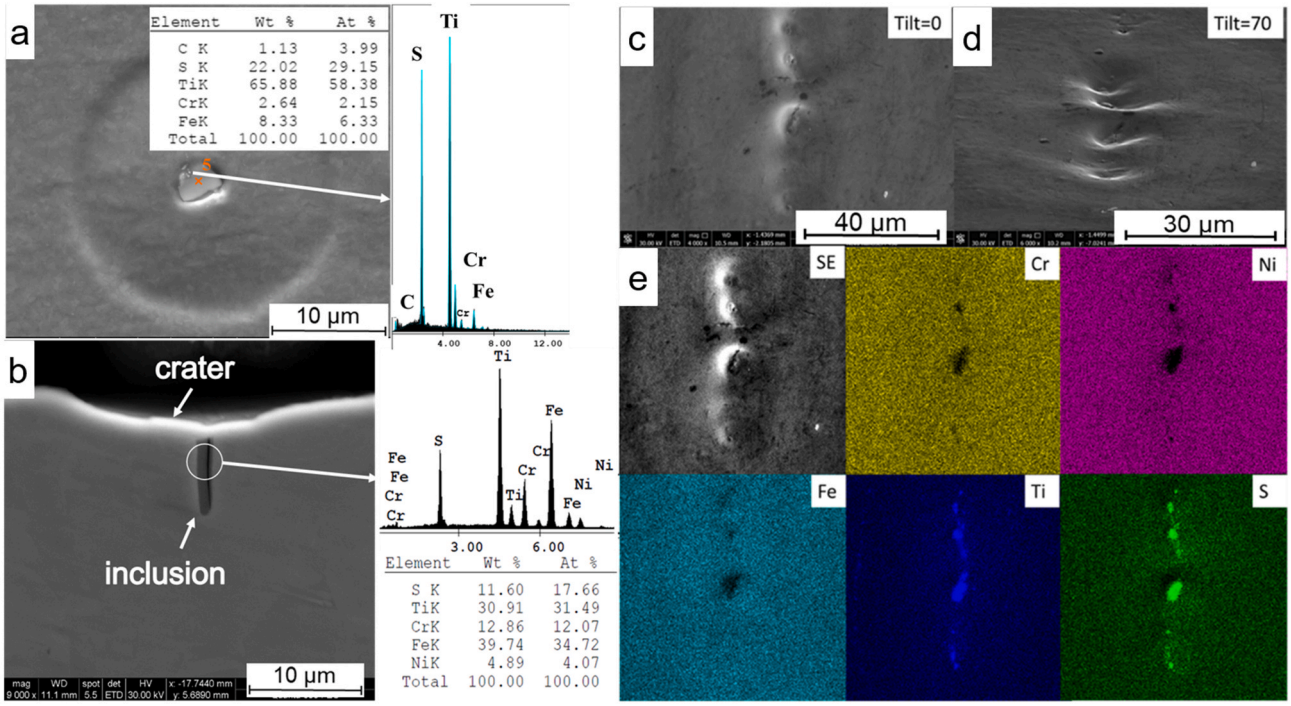

Fig. 5. SEM micrograph and elemental composition of a) a particle in the center of a crater (F = 1 J/cm^2, N = 1 pulse) and b) along the cross section of the crater (cold reduction 25%, F = 3 J/cm^2, N = 1 pulse). (c, d) images and (e) EDX maps of the elongated crater (cold reduction 50%, F = 3 J/cm^2, N = 10 pulses).

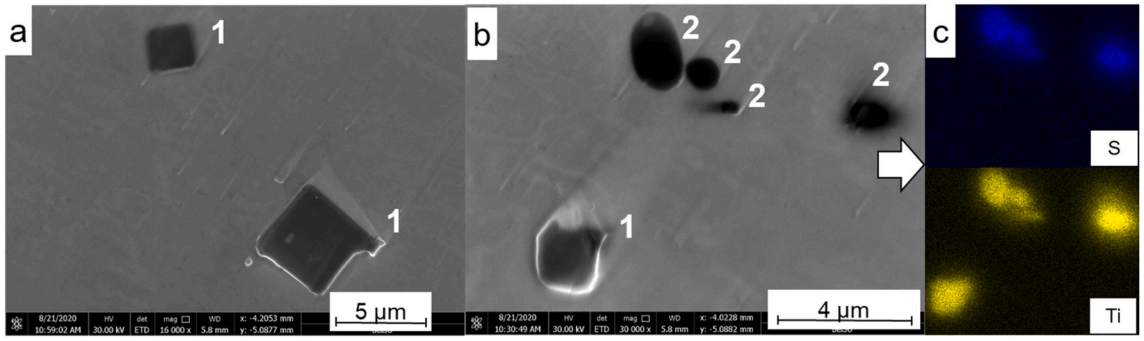

Fig. 6. SEM micrographs of inclusions in AISI 321 steel before HPIB processing(a, b) and (c) EDX maps of the distribution of sulfur (S) and titanium (Ti) in the inclusions shown in Fig. 6b. Some of the inclusions are indicated by the numbers in white, where 1 and 2 imply titanium carbides and titanium sulphides, respectively.

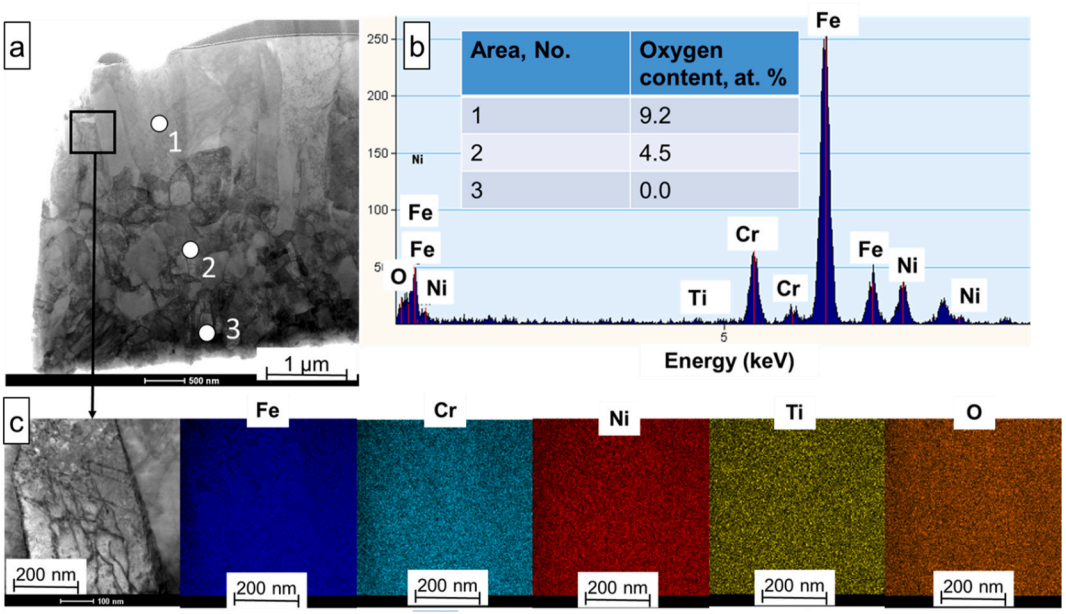

Fig. 7. a) Cross-section structure (TEM image) of the crater on AISI 321 steel (cold reduction 75%) after HPIB processing (F = 3 J/cm^2, 10 pulses). b) Oxygen content from areas 1–3 in Fig. 7a and EDX spectrum from area 1. c) EDX maps of the distribution of elements in the surface layer.

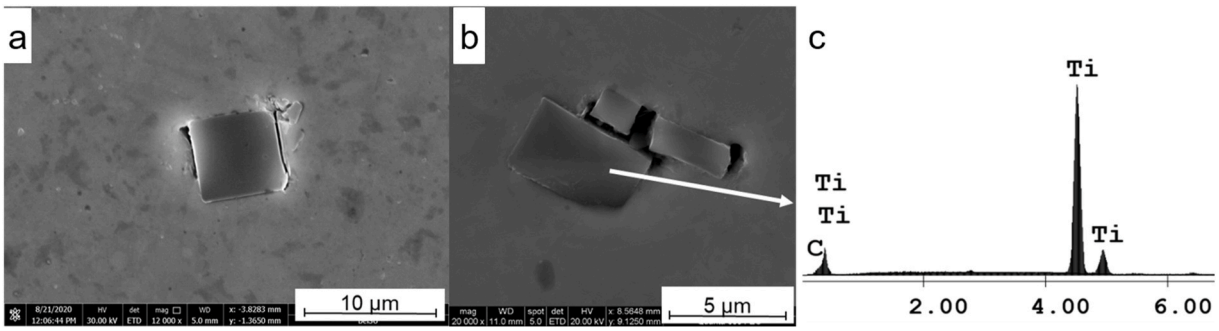

Fig. 8. (a, b) Images and (c) EDX spectrum of the titanium carbides in AISI 321 steel after HPIB processing.

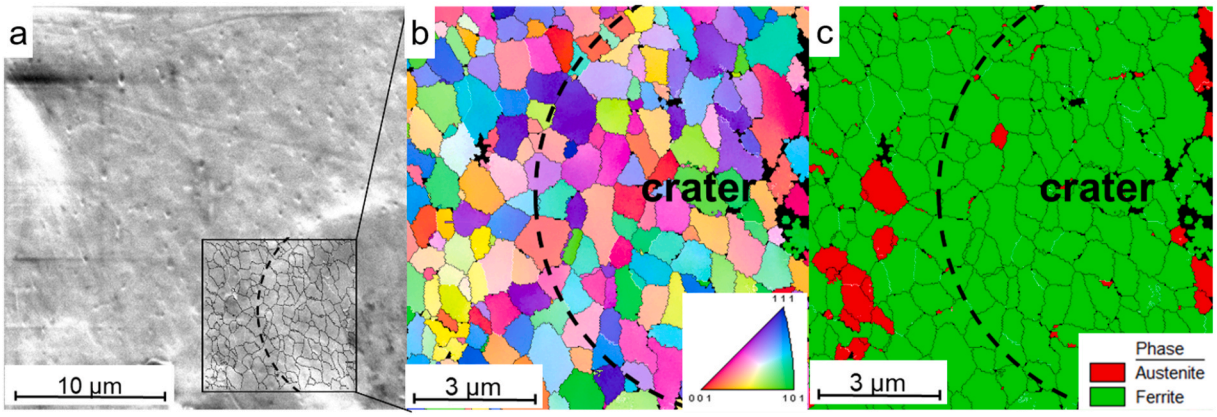

Fig. 9. Crater structure on AISI 321 steel after processing with one pulse of HPIB at F = 1 J/cm^2: (a) secondary electrons. Distribution maps of the (b) orientations and (c) phases (the black dashed line marks the crater boundary).

Fig. 4 shows the dependence of the average size of the formed craters on the initial phase composition of the target sample for a single-pulse fluence of 1 J/cm^2. The average size of the craters does not depend on the degree of preliminary deformation of the sample and its phase composition; however, craters that were elongated along the preliminary deformation direction of the sample existed on the pre-deformed sample surface along with single craters (Fig. 4b and c). Such elongated craters have been previously observed on the surface of deformed titanium alloys VT1-0 and VT6 after HPIB processing [10]. The average size of the craters decreases with a decrease in the fluence

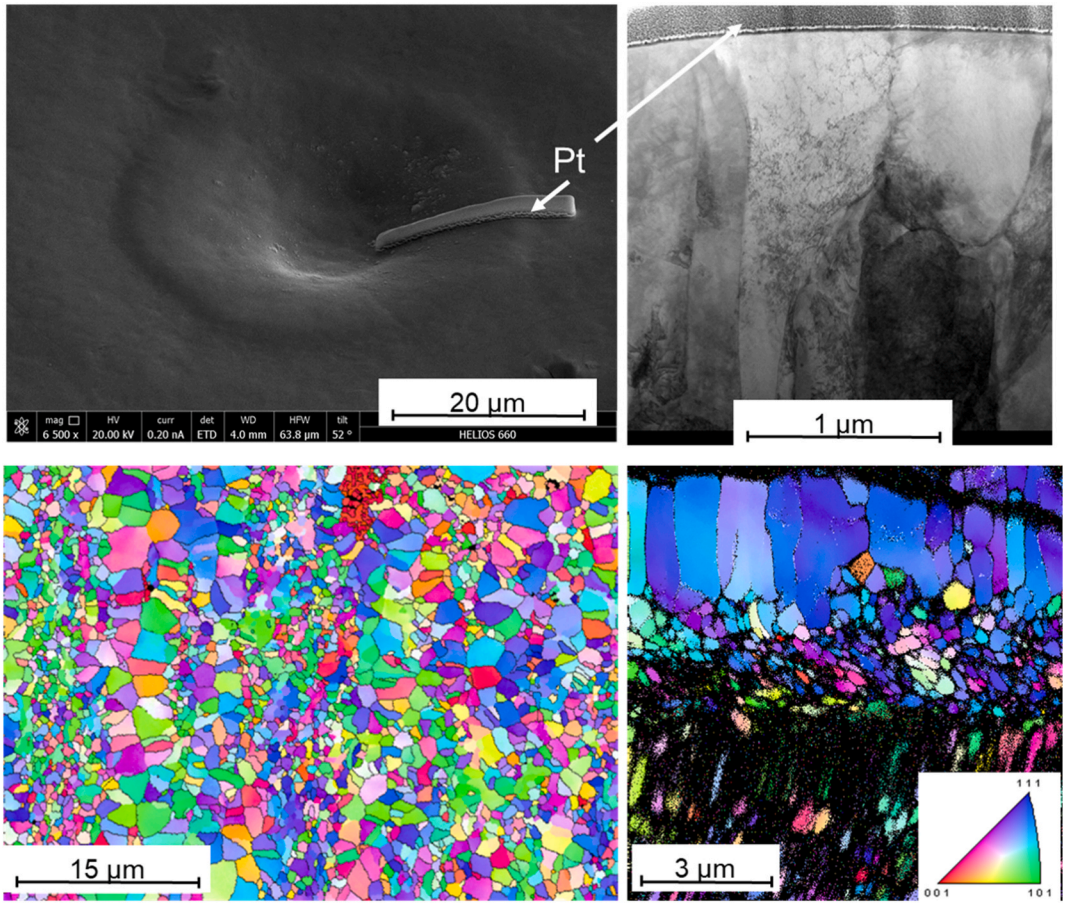

Fig. 10. a) Single crater formed on the surface of steel (cold reduction 75%) as a result of HPIB impact (F = 3 J/cm^2, 10 pulse. The sample was tilted in the microscope column by 52°. The protective platinum layer is indicated by white arrows). b) Cross-sectional structure of the same crater. c) Surface structure of the area without craters after HPIB exposure on steel (F = 3 J/cm^2, 10 pulses) and (d) its cross-section.

(Figs. 2 and 4).

3.2. Elemental composition of the crater

Typically, after HPIB processing, nonmetallic inclusions were detected in the center of craters on the surface of AISI 321 steel, which are composed of titanium and sulfur as indicated by energy dispersive analysis (Fig. 5). The inclusion in the center of the crater (Fig. 5a) has a Ti to S ratio of nearly 2:1. Regardless of the initial or deformed state of the steel and the processing parameters, the central region in all the craters that were studied contained a nonmetallic inclusion composed of titanium and sulfur (Fig. 5).

These nonmetallic inclusions were present in AISI 321 steel even before HPIB surface processing. Using SEM, we detected the following two types of inclusions in AISI 321 steel: titanium carbide or carbonitride particles (marker 1, Fig. 6) with sizes ranging from 2 to 5 μm, and 0.5–3 μm globular inclusions containing sulfur and titanium (marker 2, Fig. 6). Based on experimental results, the presence of TiC and TiCN in AISI 321 steel has been previously reported [16]. Additionally, the formation of both sulfide (TiS) and carbon sulfide ($Ti_4C_2S_2$) titanium is possible in steel [17]. The formation of Ti_2S in steel was experimentally verified [18]; however, later studies concluded that the $Ti_4C_2S_2$ phase was erroneously identified [17,19].

Therefore, we believe that the $Ti_4C_2S_2$ or TiS nonmetallic inclusions in AISI 321 steel are the preferred sites for crater formation. If the inclusions are elongated lines, for example, as a result of preliminary plastic deformation, elongated craters are formed after HPIB impact (Fig. 4b and c). Generally, a crack forms in the inclusion situated in the center of a crater or along the metal/inclusion interface. Except for the central region, the elemental composition of the crater does not differ from that of the studied steel. However, only an increased amount of oxygen was detected in the near-surface layer of the crater (Fig. 7a and b). Oxygen content in the surface-crystallized layer was about 9.2 at.%. No oxygen was detected by the TEM method for depths below 3 μm from the surface. Based on the TEM data, oxygen was uniformly distributed and did not segregate at grain boundaries (Fig. 7c). Although the pumping system in the TEMP accelerator provides a vacuum pressure greater than 0.04 Pa, surface oxidation may occur during the irradiation process. The source of oxygen and hydrogen ions can be gases (e.g., water vapor) adsorbed on the surface of an explosive-emission graphite electrode. According to the data reported in the literature [20], the ions of adsorbed gases are always present in the ion beam, and their content does not exceed 10–15%.

According to previous studies, possible mechanisms for the creation of a crater are (a) bombardment of the melted surface by the accelerator elements (a technological factor) [12,13]; (b) formation of pores in the surface layer of the sample due to casting [13]; and (c) instability in the physical and chemical states of the irradiated surface [7,12,21–24], including differences in phase and chemical composition, impurity distribution, and dislocation density of targets. Few other studies have also suggested filamentation of the ion beam in the pulse [10] and formation of a gas-plasma phase during the ablation of surface volatiles [12] as possible mechanisms for the creation of craters. All of these suggestions are still a matter of debate.

Craters induced by inclusion have often been mentioned in past studies [21–24]. The experimental data of this study are in agreement

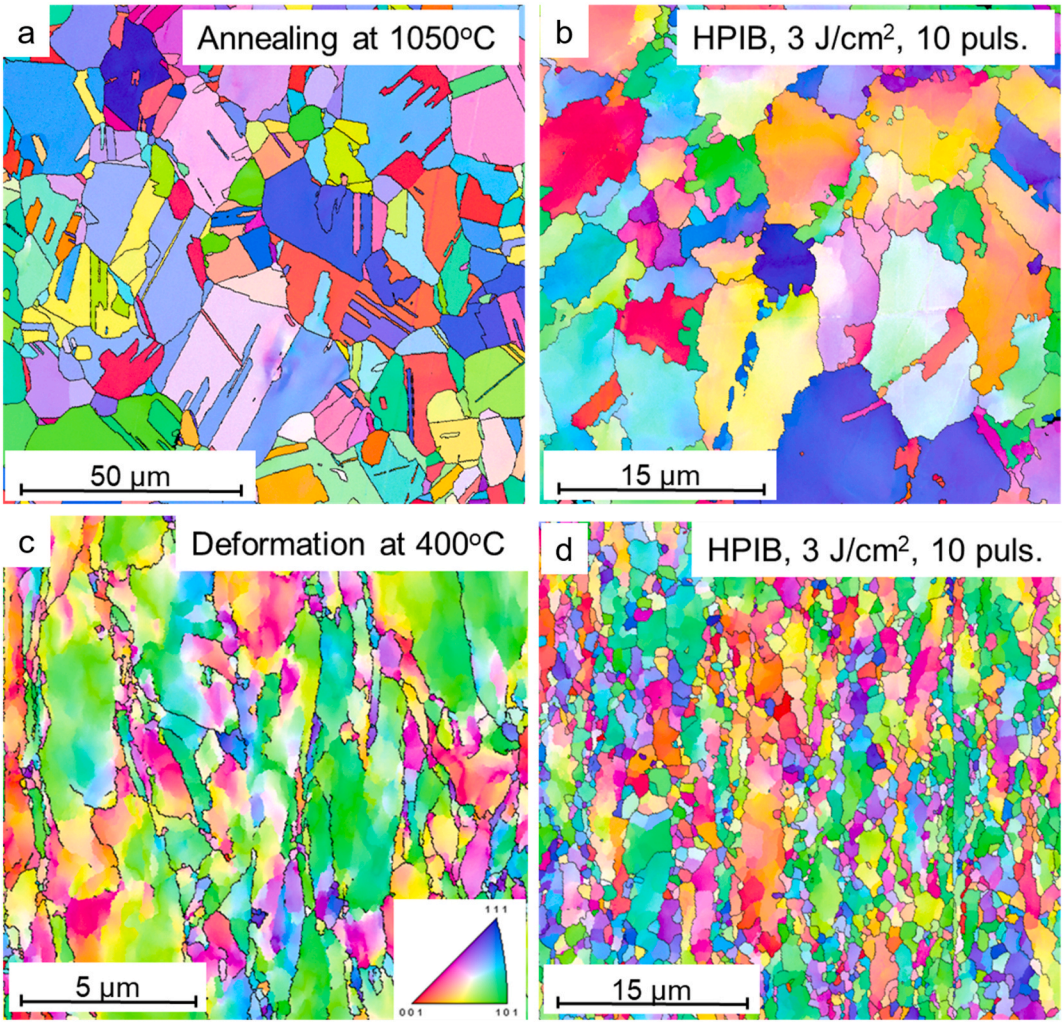

Fig. 11. Images of the AISI 321 steel structure after (a) preliminary annealing (1050 °C, 1 h), (c) deformation (rolling at 400 °C), and (b, d) subsequent processing of the surface with 10 HPIB pulses at F = 3 J/cm^2.

with previously published results [23,24]. For example [23], demonstrated that during HPIB processing (250 kV, 80 A/cm^2, 1.5 J/cm^2, 120 ns), craters (primarily consisting of Mn and S) were formed around inclusions on the surface of high-speed tool steel. It was assumed that these craters were formed as a result of the partial evaporation of a nonmetallic inclusion when the energy density of the HPIB exceeded a certain threshold value, which corresponded to the ablation threshold value of the inclusion material. In Ref. [24], it was reported that, instead of vaporization of the inclusion on the target surface, inclusions exposed to a vacuum environment can also generate craters during HPIB processing. In such a scenario, the difference in surface tensions between the molten inclusion and the molten matrix can drive the melt to flow, generating a crater on the molten target surface. In addition, the formation of microcraters on the surface was detected during the processing of steels with a low-energy-high-current electron beam (LHEB). Thus, for 304 L stainless steel [25], craters were formed mainly on the MnS inclusions after LHEB processing. It was suggested [25] that the craters were formed by the radial spreading of the melt from the localization of the MnS inclusion under the action of the surface tension gradient of the liquid melt caused by overheating of the inclusion.

According to proposed mechanisms of crater formation, a decrease in the density of craters with an increase in the number of pulses is related to the gradual dissolution of small and medium-size inclusions. Craters formed around large inclusions are likely to be larger than those formed around smaller inclusions. Therefore, an increase in the average size of the craters is related both to the size of the inclusion and to the merging of separate craters.

The titanium carbides or carbonitrides in AISI 321 steel are not crater sites. This may be due to the difference in thermal properties of titanium carbide and titanium sulfide. However, as a result of HPIB impact, cracks can form at the particle/metal interface or the inclusions can be destroyed (Fig. 8). Formation of cracks can therefore also be associated with the thermal stresses arising during rapid cooling (10^9–10^{10} K/s) of the heated surface.

3.3. Crater structure

EBSD analysis of the crater area on the steel surface was performed after impacting it with an 1 J/cm^2 fluence HPIB pulse (see Fig. 9, the crater area is highlighted by a black dashed line). It should be noted that the structure and phase composition of the entire crater surface do not differ from those of the nearby surface regions outside the crater boundaries. Similar results were observed when the steel surface was irradiated by HPIB with a fluence of 3 J/cm^2, both for single-pulse and multipulse processing.

Examination of the structure of a single crater through transmission electron microscopy revealed that in the near-surface layer of the crater (Fig. 10a), the crystallites elongated toward the surface with a large coefficient of grain nonuniformity (Fig. 10b). However, additional studies of the cross-section of the sample showed similar crystallites in

the near-surface layers of the regions that were without craters (Fig. 10c and d).

The obtained results indicate that the structure-forming processes in the crater and the areas without craters occur simultaneously after HPIB impact. These data do not contradict the mechanism proposed in a previous study [13], according to which the surface layer and inclusions (sulfides) melt due to HPIB impact and the resulting crater is caused by melt flow due to the difference in the surface tension coefficients of the matrix and inclusions. Moreover, the preliminary results indicate that the formation of the structure on the surface layer of AISI 321 steel after exposure to HPIB is significantly influenced not only by the processing parameters of the HPIB but also by the initial structure of the material being processed. Fig. 10 displays images of the structure of the steel samples preliminarily subjected to various types of thermomechanical processing followed by HPIB processing with the same irradiation parameters ($F = 3$ J/cm^2, 10 pulses). According to Ref. [24], the formation of craters indicates melting of the surface layer. However, as shown in Fig. 11, the final structures after HPIB irradiation of the annealed (Fig. 11a and b) and plastically deformed (Fig. 11c and d) samples are significantly different, which cannot be explained by the processes of melting and subsequent ultrafast crystallization alone. The features of the formed structure indicate that one of the structure-forming processes in the near-surface layers after the HPIB impact is recrystallization and the migration of the high-angle grain boundaries. As a result of HPIB impact, Σ3 twin boundaries, which are commonly observed in austenitic steel, were almost absent. Moreover, after the HPIB processing of the steel in the initial state (without plastic deformation), curved high-angle grain boundaries, possibly due to their migration, could be observed (Fig. 11b). For the plastically deformed sample, characterized by a high proportion of low-angle grain boundaries and elongated grains along the rolling direction (Fig. 11c), HPIB impact leads to the formation of a predominantly equiaxed fine-grained structure in the near-surface layers (Fig. 11d)).

4. Conclusions

1. Irradiation of austenitic stainless steel with HPIB leads to the formation of craters mainly around nonmetallic inclusions (titanium sulfides or carbosulfides).
2. With an increase in the number of impact impulses, the number of craters decreases and their average size increases.
3. The number of craters formed on AISI 321 steel and their average size are not dependent on the austenite/ferrite phase ratio before surface processing.
4. The structure and phase composition of the crater surface and those of the nearby surface regions outside the crater boundaries are the same.

Declaration of competing interest

The authors declare that they have no known competing financial interests or personal relationships that could have appeared to influence the work reported in this paper.

Acknowledgements

This study was funded by Russian Foundation for Basic Research, project number 20-08-00907.

References

[1] V.A. Shulov, N.A. Nochovnaya, G.E. Remnev, Termomechanical processing of titanium alloys by high power pulsed ion beams, Mater. Sci. Eng. A 243 (1998) 290–293, https://doi.org/10.1016/s0921-5093(97)00816-2.
[2] X. Ma, G. Zhang, G. Wang, G. Zhu, W. Zhou, J. Wang, B. Sun, Surface morphology, microstructure and properties of as-cast AZ31 magnesium alloy irradiated by high intensity pulsed ion beams, Appl. Surf. Sci. 311 (2014) 567–573, https://doi.org/10.1016/j.apsusc.2014.05.109.
[3] X. Wang, M.K. Lei, J.S. Zhang, Surface modification of 316L stainless steel with high-intensity pulsed ion beams, Surf. Coating. Technol. 201 (2007) 5884–5890, https://doi.org/10.1016/j.surfcoat.2006.10.040.
[4] V.A. Shulov, N.A. Nochovnaia, G.E. Remnev, The effect of crater creation on the fatigue strength and corrosion resistance of steels and titanium alloys irradiated by high-power pulsed ion beams, Surf. Coating. Technol. 158–159 (2002) 488–493, https://doi.org/10.1016/S0257-8972(02)00299-2.
[5] D.J. Rej, H.A. Davis, M. Nastasi, J.C. Olson, E.J. Peterson, R.D. Reiswig, K. C. Walter, R.W. Stinnett, G.E. Remnev, V.K. Struts, Surface modification of AISI-4620 steel with intense pulsed ion beams, Nucl. Instrum. Methods Phys. Res. Sect. B Beam Interact. Mater. Atoms 127 (1997) 987–991, https://doi.org/10.1016/S0168-583X(97)00044-X.
[6] B.P. Wood, A.J. Perry, L.J. Bitteker, W.J. Waganaar, Cratering behavior in singleand poly-crystalline copper irradiated by an intense pulsed ion beam, Surf. Coating. Technol. 108 (1998) 171–176, https://doi.org/10.1016/S0257-8972(98)00659-8.
[7] G.V. Potyomkin, A.E. Ligchev, M.V. Zhidkov, Y.R. Kolobov, G.E. Remnev, M. Y. Gazizova, S.A. Bozhko, S.K. Pavlov, The change in the surface topography of magnesium under high-flux C ion radiation, J. Phys.: Conf. Ser. 652 (2015), 012005, https://doi.org/10.1088/1742-6596/652/1/012005.
[8] X.P. Zhu, M.K. Lei, Z.H. Dong, S.M. Miao, T.C. Ma, Crater formation on the surface of titanium irradiated by a high-intensity pulsed ion beam, Surf. Coating. Technol. 173 (2003) 105–110, https://doi.org/10.1016/S0257-8972(03)00321-9.
[9] V.A. Shulov, N.A. Nochovnaya, Crater formation on the surface of metals and alloys during high power ion beam processing, Nucl. Instrum. Methods Phys. Res. Sect. B Beam Interact. Mater. Atoms 148 (1999) 154–158, https://doi.org/10.1016/j.surfcoat.2006.01.078.
[10] M.V. Zhidkov, A.E. Ligachev, Y.R. Kolobov, G.V. Potemkin, G.E. Remnev, Effect of high-power ion beams on the surface topography and structure of the subsurface layer of submicrocrystalline titanium alloys, Russ. J. Non-Ferrous Metals 60 (2019) 590–597, https://doi.org/10.3103/S1067821219050195.
[11] X. Yu, J. Shen, H. Zhong, J. Zhang, S. Yan, G. Zhang, X. Zhang, X. Le, Thermo-hydrodynamic process simulation of craters formation and evolution on metal surfaces caused by intense pulsed ion beams, Vacuum 120 (2015) 116–120, https://doi.org/10.1016/j.vacuum.2015.06.028.
[12] V.A. Shulov, A.S. Novikov, A.G. Paikin, A.B. Belov, A.F. Lvov, G.E. Remnev, Crater formation on the surface of refractory alloysduring high-power ion-beam processing, Surf. Coating. Technol. 201 (2007) 8654–8658, https://doi.org/10.1016/j.surfcoat.2006.01.078.
[13] S. Yan, X.Y. Le, W.J. Zhao, J.M. Xue, Y.G. Wang, A possible thermodynamic mechanism of craters formation on metal surfaces caused by intense pulsed ion beams, Surf. Coating. Technol. 193 (2005) 69–74, https://doi.org/10.1016/j.surfcoat.2004.07.063.
[14] A. Pardo, M.C. Merino, A.E. Coy, F. Viejo, M. Carboneras, R. Arrabal, Influece of Ti, C and N concentration on the intergranular corrosion behaviour of AISI 316Ti and 321 stainless steels, Acta Mater. 55 (2007) 2239–2251, https://doi.org/10.1016/j.actamat.2006.11.021.
[15] G.E. Remnev, V.A. Shulov, Application of high-power ion beams for technologylaser part, Beams 11 (1993) 707–731, https://doi.org/10.1017/S0263034600006467.
[16] S.S. Kasana, O.P. Pandey, Effect of heat treatment on microstructure and mechanical properties of boron containing Ti-Stabilized AISI-321 steel for nuclear power plant application, Mater. Today Commun. 26 (2021), 101959, https://doi.org/10.1016/j.mtcomm.2020.101959.
[17] P.R. Wilson, Z. Chen, TEM characterization of iron titanium sulphide intitanium- and niobium-containing low manganese steel, Scripta Mater. 56 (2007) 753–756, https://doi.org/10.1016/j.scriptamat.2007.01.020.
[18] W.R. Bandi, G. Krap, Identification and determination of TitaniumSulphide and carbosulphidle compounds in steel, Analyst 104 (1979) 812, https://doi.org/10.1039/an9790400812.
[19] C.J. Ball, X-ray powder diffraction patterns of titanium carbosulphide and τ titanium sulphide, Met. Sci. 18 (1984) 577, https://doi.org/10.1179/030634584790419674.
[20] I.F. Isakov, V.N. Kolodii, M.S. Opekunov, V.M. Matvienko, S.A. Pechenkin, G. E. Remnev, Yu P. Usov, Sourses of high power ion beams for technological applications, Vacuum 42 (1991) 159–162, https://doi.org/10.1016/0042-207X(91)90101-N.
[21] V.S. Kovivchak, T.V. Panova, K.A. Mikhailov, E.V. Knyazev, Features of the surface morphology of brass and bronze upon irradiation with a high power ion beam, J. Surf. Invest.: X-ray, Synchrotron Neutron Tech. 7 (2013) 531–535, https://doi.org/10.1134/S1027451013020365.
[22] X.P. Zhu, M.K. Lei, Z.H. Dong, S.M. Miao, T.C. Ma, Crater formation on the surface of titanium irradiated by a high-intensity pulsed ion beam, Surf. Coating. Technol. 173 (2003) 105–110, https://doi.org/10.1016/S0257-8972(03)00321-9.
[23] H. Zhong, J. Zhang, J. Shen, X. Yu, G. Liang, X. Cui, X. Zhang, G. Zhang, S. Yan, X. Le, Craters forming mechanism of high speed steel irradiated by intense pulsed ion beam, Nucl. Instrum. Methods Phys. Res. Sect. B Beam Interact. Mater. Atoms 409 (2017) 298–301, https://doi.org/10.1016/j.nimb.2017.04.002.
[24] H. Zhong, J. Zhang, J. Shen, G. Liang, Sh Zhang, M. Xu, X. Yu, S. Yan, G.E. Remnev, X. Le, Dynamic mechanism of crater formation induced by inclusion during intense pulsed ion beam irradiation, Vacuum 179 (2020), 109541, https://doi.org/10.1016/j.vacuum.2020.109541.
[25] G.E. Ozur, D.I. Proskurovsky, V.P. Rotshtein, A mechanism of microcrater formation in metallic material irradiated by a low-energy high-current electron

beam, Tech. Phys. Lett. 42 (2016) 328–331, https://doi.org/10.1134/S1063785016030275.